RSC Advances

PAPER

View Article Online
View Journal | View Issue



Cite this: *RSC Adv.*, 2026, **16**, 7936

# Dual-activated fluorescent probe for the study of the mechanism of $SO_2$ and NO in cisplatin resistance of nasopharyngeal carcinoma

Xiaofeng Wang, [a] Xinyu Li,[b] Xiaoqiang Chen*[a] and Desheng Wang*[a]

Cisplatin is widely used in the treatment of advanced nasopharyngeal carcinoma; however, its therapeutic application is often limited by a high incidence of drug resistance. Recent studies have demonstrated that nitric oxide (NO) and sulfur dioxide ($SO_2$), acting as gaseous signaling molecules, exhibit anti-cisplatin resistance properties in tumor cells. Nevertheless, developing appropriate chemical tools to investigate the mechanisms underlying NO and $SO_2$ mediated cisplatin resistance to cisplatin remains challenging. This study designed and synthesized a dual-responsive fluorescent probe to detect peroxynitrite ($ONOO^-$) and $SO_2$, enabling them to be visualized within cells. Using this probe to detect and image $ONOO^-$ and $SO_2$ in cisplatin-resistant cell lines revealed that NO and $SO_2$ combat cisplatin resistance by generating highly reactive $ONOO^-$ and depleting intracellular glutathione. The $IC_{50}$ values of cisplatin-resistant cells treated with NO and $SO_2$ were significantly lower than those of the control group. These results indicate that HCy–$ONOO^-$–$SO_2$ can serve as a powerful chemical tool for investigating the mechanisms of cisplatin resistance in nasopharyngeal carcinoma.

Received 28th October 2025
Accepted 30th January 2026

DOI: 10.1039/d5ra08282j

rsc.li/rsc-advances



## 1. Introduction

Nasopharyngeal carcinoma (NPC) is a malignant tumor that originates in the epithelium of the nasopharynx, often appearing in the pharyngeal recess.[1] Due to its unique anatomical location, the early symptoms of NPC are not obvious. Among patients presenting for the first time with NPC, more than 70% have locally advanced nasopharyngeal carcinoma.[2–4] Therefore, chemotherapy plays a crucial role in NPC treatment, particularly in R/M NPC cases.[5–7]

Cisplatin (also known as DDP) is a widely used platinum-based chemotherapeutic agent in clinical practice. It has become a cornerstone in the treatment of various solid tumors, including NPC, ovarian cancer, bladder cancer, lung cancer, and colorectal cancer.[8,9] However, many tumors that initially respond to cisplatin gradually develop resistance during treatment, significantly limiting its clinical efficacy.[10,11] Due to the non-specific interactions between cisplatin and intracellular components, as well as the various mechanisms through which cisplatin induces DNA damage and apoptosis, tumor cells can acquire resistance *via* multiple molecular pathways.[12,13] Numerous studies have demonstrated that inhibiting ATPase activity and reducing intracellular cisplatin efflux are effective strategies to enhance cisplatin sensitivity. Following its hydrolysis in the cytoplasm, cisplatin readily binds to sulphur-containing intracellular molecules, such as glutathione (GSH), sequestering the drug in the cytoplasm and preventing its translocation to the nucleus for DNA binding. Consequently, depleting intracellular GSH is another viable approach to increasing cisplatin chemosensitivity.

Gaseous messenger small molecules are a type of gas molecules produced by metabolism within the body and play an important role in signal transduction under normal physiological and pathological conditions. Studies have shown that nitric oxide (NO), an important gaseous messenger, can overcome the multidrug resistance in tumor cells by reducing *P*-glycoprotein expression and increasing sensitivity to chemotherapy. NO interacts with superoxide anion free radicals to generate highly reactive peroxynitrite ($ONOO^-$), which can inhibit the mitochondrial respiratory chain and lead to mitochondrial dysfunction and the oxidation of ATPase.[14] Therefore, the ability of NO to reduce intracellular cisplatin efflux and enhance the killing effect of cisplatin on mitochondria in order to overcome cisplatin resistance by generating $ONOO^-$ requires further exploration. On the other hand, once hydrolysed in the cytoplasm, cisplatin is prone to binding with intracellular sulphur-containing molecules such as GSH, thereby preventing it from entering the nucleus and binding to its target DNA. Therefore, depleting intracellular GSH is also a way to increase sensitivity to cisplatin.

In conclusion, monitoring intracellular levels of $ONOO^-$ and sulfur dioxide ($SO_2$) is crucial for studying the role and mechanism of $SO_2$/NO in anti-cisplatin resistance. The high

[a]*Department of Otolaryngology, The Affiliated Union Hospital, Fujian Medical University, No. 29, Xinquan Road, Fuzhou, 350001, China. E-mail: cxq7177223446@163.com; wangds@fjmu.edu.cn*

[b]*Jinan Vocational College, No. 5518, Lvyou Road, Jinan City, 250100, China*

sensitivity, selectivity, and spectral characteristics of small-molecule fluorescent probes make them indispensable tools in modern analytical chemistry and biomedical research.[15–17] Furthermore, the use of these probes in biological imaging and *in vivo* monitoring enables researchers to observe the dynamic molecular changes in the body in real time. However, most probes cannot conduct separate and simultaneous detection without interference. Based on previous studies, this research has innovatively developed a small molecule fluorescent probe for the first time that can simultaneously detect and image $ONOO^-$ and $SO_2$. Using the developed $ONOO^-$ and $SO_2$ small molecule fluorescent probes, the anti-cisplatin resistance effect and mechanism of $NO/SO_2$ in NPC were explored.

## 2. Materials and methods

### 2.1. Materials

All organic synthetic materials are of analytical grade, while and all cell reagents are of biological grade. The organic synthetic reagents were purchased from Energy Chemical in Anhui, China. Normal nasopharyngeal cells (NP69) were purchased from the Xiang Ya Central Experiment Laboratory in Changsha, China. NPC cells (C666-1) were purchased from Fuheng Biology in Shanghai, China. DMSO (BL165B), CCK-8 (BS350B), RPMI-1640 (PM150110) and Typsin-EDTA Solution (BL501A) were purchased from Biosharp in Anhui, China. Fetal bovine serum (S660JY) was purchased from Basalmedia (Shanghai, China). The Reduced Glutathione Content Assay Kit (BC1175) was purchased from Solarbio, Beijing, China.

### 2.2. Construction of cisplatin-resistant cells

First, a stable *in vitro* model was obtained through the traditional continuous culture method. By continuously culturing the NPC cell line C666-1 for 6 months and gradually increasing the cisplatin dose to 4 μmol $mL^{-1}$, we established a cisplatin-resistant NPC cell line (C666-1/DDP). The drug concentration escalation method[18] was employed. C666-1 cells in logarithmic growth phase were treated with low-concentration DDP for 24 h, followed by medium replacement. After cell recovery, the cells were digested and subcultured, then re-exposed to low-concentration cisplatin for 24 hours. When cells reached normal morphology, the drug shock protocol was repeated 6–8 times at each concentration (0 μmol $mL^{-1}$, 1 μmol $mL^{-1}$, 2 μmol $mL^{-1}$, 3 μmol $mL^{-1}$ and 4 μmol $mL^{-1}$). Once stable growth was achieved, the drug concentration was gradually increased during subsequent cultures. The drug induction period lasted 6 months until cells could grow stably in 4 μmol $L^{-1}$ DDP. CCK-8 assay was used to evaluate the resistance index (RI) of drug-resistant and parental strains, with RI > 5 indicating drug resistance.

## 3. Results and discussion

### 3.1. Design and synthesis of HCy–$ONOO^-$–$SO_2$

Fig. S1 shows the preparation method of the probe. Under ice bath conditions and in an argon atmosphere, HCy (217 mg, 0.5 mmol) was dissolved in 10 mL of anhydrous $CH_2Cl_2$, followed by the addition of 50 μL of piperidine. A dropwise addition was then performed of a solution of 236 mg (2 mmol) solution of diphenylphosphine oxychloride in 5 mL of dichloromethane was performed. The reaction was maintained at room temperature for 6 hours after an initial one-hour incubation period. Fig. S1 shows the preparation method of the probe.

Dissolve HCy (217 mg, 0.5 mmol) in 10 mL anhydrous $CH_2Cl_2$ in an ice bath and argon atmosphere, and then add 50 μL of piperidine. Subsequently, add dropwise a solution of diphenylphosphine oxychloride (472 mg, 2 mmol) dissolved in 5 mL of dichloromethane. After stirring for 1 h in an ice bath, return to room temperature and continue the reaction for another 6 h. The solvent was then removed and the product purified by column chromatography ($CH_2Cl_2$ : $CH_3OH$ = 30 : 1, v/v), yielding the final compound HCy–$ONOO^-$–$SO_2$ (117 mg, yield 37%). As shown in Fig. S3–S5, the structure of the probe was verified. $^1$H NMR (400 MHz, DMSO-$D_6$) $\delta$ 8.45 (dd, $J$ = 16.2, 8.4 Hz, 1H), 8.36 (t, $J$ = 7.9 Hz, 1H), 8.30–8.22 (m, 2H), 8.22–8.10 (m, 5H), 7.95–7.93 (m, 1H), 7.92–7.90 (m, 1H), 7.84–7.71 (m, 2H), 7.67 (ddd, $J$ = 11.1, 7.4, 2.1 Hz, 2H), 7.63–7.43 (m, 6H), 6.94–6.91 (m, 1H), 4.95–4.87 (m, 2H), 2.67 (t, $J$ = 6.1 Hz, 2H), 2.19 (d, $J$ = 9.9 Hz, 2H), 1.96 (d, $J$ = 6.9 Hz, 6H). $^{13}$C NMR (400 MHz, DMSO-$D_6$) 182.95, 163.85, 154.25, 152.23, 138.99, 133.57, 133.35, 132.18, 132.08, 131.49, 130.57, 129.66, 129.53, 128.85, 127.27, 126.77, 123.72, 123.52, 121.75, 116.94, 113.62, 112.70, 109.12, 54.37, 53.91, 47.77, 26.30, 25.87, 25.20. HRMS *m*/*z*: calculated for [$C_{37}H_{34}NO_5PS$]: 635.1895, found [$C_{37}H_{34}NO_5PS$ + H]$^+$: 636.1952. Furthermore, we measured the infrared spectrum of the compound HCy–$ONOO^-$–$SO_2$ (Fig. S7). These characteristic absorption bands are consistent with the presence of an extended aromatic conjugated system, phosphate ester moieties, and sulfonate groups, confirming the successful formation of the target compound HCy–$ONOO^-$–$SO_2$.

Scheme 1 shows the structure of the probe HCy–$ONOO^-$–$SO_2$ and how it reacts with $SO_2$ and $ONOO^-$. This semi-carbocyanine compound has excellent spectral properties and is widely used in the fields of biomedical science, dye-sensitized science and environmental science, making it a recommended luminescent group.[19,20] Due to the presence of the indole cation, HCy–$ONOO^-$–$SO_2$ can accumulate effectively at mitochondrial sites. To further improve the probe's water solubility, we introduced a sulfonic acid group alongside the indole cation, which significantly enhances its biocompatibility. Recent studies have found that the diphenylphosphinoyl ester group exhibits a rapid response, excellent sensitivity, and remarkable selectivity towards $ONOO^-$.[21,22] Based on this, we selected the diphenylphosphinoyl ester group as the specific $ONOO^-$ trigger in this design. Its introduction inhibits the probe's intramolecular charge transfer process, resulting in inert fluorescence. In the presence of $ONOO^-$, HCy–$ONOO^-$–$SO_2$ generates a strong fluorescence signal at 575 nm within 10 minutes. Furthermore, under $SO_2$ conditions, a Michael addition reaction occurs, disrupting the large conjugated system and leading to enhanced fluorescence at 450 nm within 15 minutes. Therefore, this probe can be used to detect of $SO_2$ and $ONOO^-$ separately through distinct signals, providing a solid basis for studying their interrelationships.

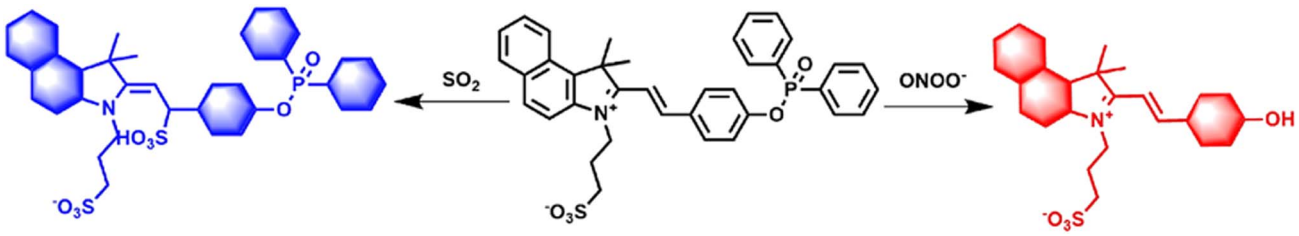


Scheme 1 The molecular structure of HCy–$ONOO^-$–$SO_2$ and its reaction mechanisms with $ONOO^-$ and $SO_2$.

### 3.2. Spectral characterization of the probe for $ONOO^-$ and $SO_2$

First, the spectral properties of HCy–$ONOO^-$–$SO_2$ were investigated in phosphate buffer solution. A detailed analysis of the ultraviolet-visible (UV-vis) absorption spectral changes of the HCy–$ONOO^-$–$SO_2$ probe was conducted. As can be seen in Fig. S7, the probe exhibits a distinct absorption band around 450 nm. The addition of $ONOO^-$ results in the emergence of a stronger absorption peak at 460 nm, indicating the formation of a new product from the reaction between the probe and $ONOO^-$. Conversely, in the presence of $SO_2$, HCy–$ONOO^-$–$SO_2$ exhibits a new absorption band at 315 nm while the original absorption peak at 450 nm disappears completely. This distinct spectral response demonstrates that HCy–$ONOO^-$–$SO_2$ can effectively detect $SO_2$. Furthermore, in the presence of both $SO_2$ and $ONOO^-$, the probe exhibits a strong absorption band at approximately 315 nm and weak absorption features around 460 nm, while the original absorption peak at 450 nm disappears completely. These results demonstrate the potential of HCy–$ONOO^-$–$SO_2$ for use in the detecting of $ONOO^-$ and $SO_2$ under co-existing conditions.

In addition, the fluorescence spectral changes of $ONOO^-$ and $SO_2$ in the HCy–$ONOO^-$–$SO_2$ system were investigated systematically. As illustrated in Fig. 1A, the addition of $ONOO^-$ resulted in a progressive increase in the fluorescence signal of HCy–$ONOO^-$–$SO_2$ at 585 nm with increasing concentration. This indicates that the probe can effectively monitor variations in $ONOO^-$ levels. In the presence of $SO_2$, a gradual enhancement of the fluorescence signal at 465 nm was observed (Fig. 1B), which further demonstrates the potential of this probe for $SO_2$ detection. Furthermore, a strong linear correlation was established between fluorescence intensity and the concentrations of $ONOO^-$ and $SO_2$. The calibration curves were described by the following equations: $Y_1 = 64.1584X + 87.9061$ ($R^2 = 0.9994$) for $ONOO^-$ and $Y_2 = 28.4919X + 151.7518$ ($R^2 = 0.9996$) for $SO_2$ (Fig. 1C and D).

To evaluate the probe's ability to detect $ONOO^-$ and $SO_2$ *in vivo*, we examined how pH affects the fluorescence response of HCy–$ONOO^-$–$SO_2$. As illustrated in Fig. S9A and B, HCy–$ONOO^-$–$SO_2$ exhibits a stable and minimal fluorescence signal across the pH range of 4 to 9, indicating that the probe's performance remains unaffected by physiological pH variations. In contrast, the presence of $ONOO^-$ and $SO_2$ causes HCy–$ONOO^-$–$SO_2$ to generate distinct fluorescence emissions at 575 nm and 450 nm, respectively, within the physiologically relevant pH range of 4–7. Next, we investigated the response kinetics of HCy–$ONOO^-$–$SO_2$ towards $ONOO^-$ and $SO_2$. As illustrated in Fig. S9C, the fluorescence signal of HCy–$ONOO^-$–$SO_2$ reached its maximum within approximately 10 min upon addition of $ONOO^-$, indicating a rapid response to $ONOO^-$. As shown in Fig. S9D, when exposed to different $SO_2$ concentrations, the fluorescence intensity reached saturation within approximately 15 min, demonstrating that the probe is also effective for $SO_2$ detection. Notably, the distinct reaction kinetics of the probe towards $ONOO^-$ and $SO_2$ enable discrimination between the two, offering potential for selective and sequential detection. These results suggest that HCy–$ONOO^-$–$SO_2$ can be used for the *in vivo* monitoring of both $ONOO^-$ and $SO_2$. Additionally, we examined the fluorescence responses of this probe to various reactive species, amino acids, and common anions. As shown in Fig. 1E and F, $ONOO^-$ and $SO_2$ produced distinct fluorescence enhancements at 575 nm and 450 nm, respectively, no significant changes in signal were observed in the presence of the other tested substances. These findings demonstrate the high selectivity of HCy–$ONOO^-$–$SO_2$ towards $ONOO^-$ and $SO_2$ in complex biological environments.

### 3.3. Visualization of $ONOO^-$ and $SO_2$ in living cells

Subsequently, the cytotoxicity and biocompatibility of the probe HCy–$ONOO^-$–$SO_2$ were evaluated using the CCK-8 assay. As shown in Fig. S10, the cells exhibited high viability even at elevated probe concentrations, indicating that the designed probe exhibits low cytotoxicity and favorable biocompatibility. To evaluate the probe's ability to detect $ONOO^-$ and $SO_2$ in living cells, we used it to visualise and image these species in the normal nasopharyngeal cells (NP69). As shown in Fig. 2A and B, no fluorescence was observed in the absence of $ONOO^-$ and $SO_2$. However, upon exposure to $ONOO^-$ and $SO_2$, a strong red fluorescence signal was detected in NP69 cells after 20 min, indicating that HCy–$ONOO^-$–$SO_2$ can detect $ONOO^-$ in cellular environments. However, as the incubation time increased, the blue fluorescence intensity increased while the red fluorescence gradually diminished within 10 min. We hypothesise that this phenomenon may be attributed to $SO_2$ disrupting the extended conjugated system, which reduces the red fluorescence signal while enhancing the blue fluorescence signal. This study demonstrates that dual-target detection of $ONOO^-$ and $SO_2$ can be achieved by monitoring the temporal evolution of dual fluorescence signals.

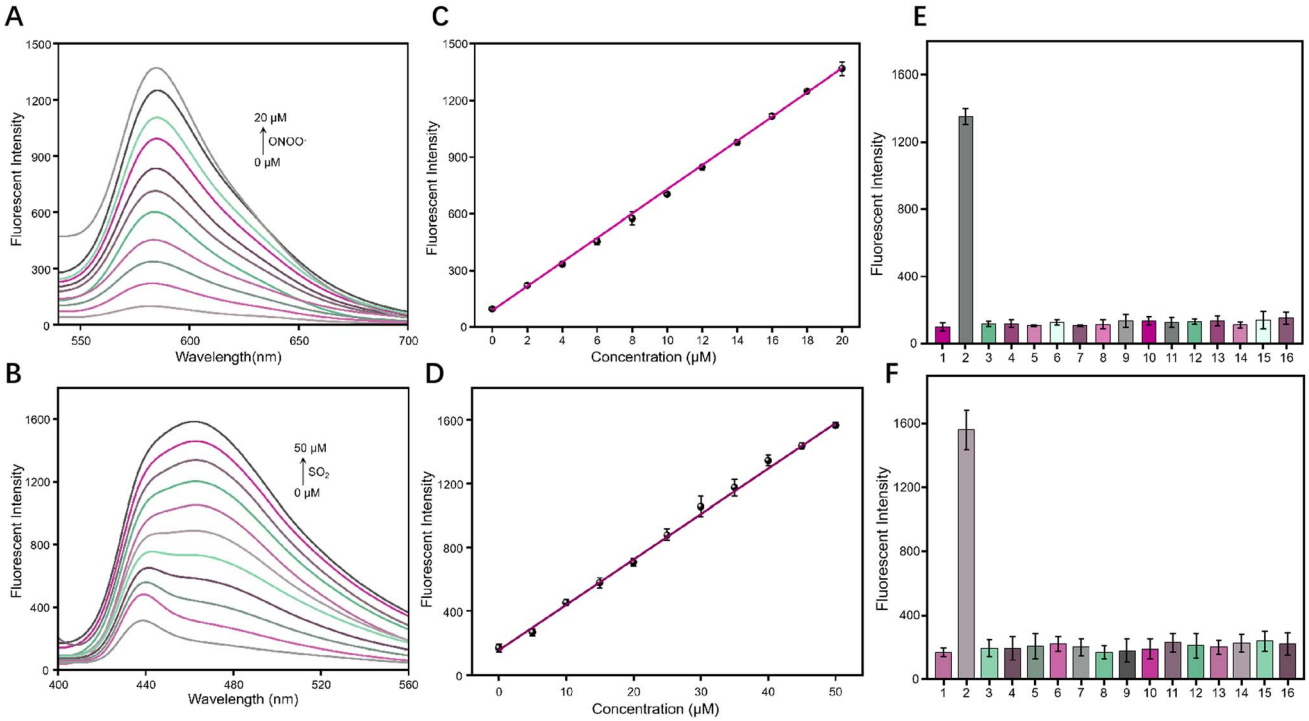


Fig. 1 Spectral properties of HCy–$ONOO^-$–$SO_2$ in the presence of $ONOO^-$ and $SO_2$. Fluorescence emission spectra were recorded in PBS buffer (10 mM, pH 7.4, PBS : DMSO = 19 : 1 v/v). (A) Fluorescence response of HCy–$ONOO^-$–$SO_2$ to $ONOO^-$ (0–20 μM) was measured at an excitation wavelength of 575 nm, and data were collected after a 10 min incubation. (B) Response to $SO_2$ (0–50 μM) was monitored at an excitation wavelength of 450 nm under the same instrumental conditions, with a 20 min incubation period. (C) and (D) Linear calibration curves for $ONOO^-$ (0–20 μM) and $SO_2$ (0–50 μM), respectively, showing the quantitative relationship between fluorescence intensity and analyte concentration. (E) and (F) The probe exhibited distinct emission signals for different species, which were recorded at (E) 575 nm and (F) 450 nm. (E) (1) blank; (2) $ONOO^-$ (20 μM); (3) $HPO_4^{2-}$ (500 μM); (4) $PO_4^{3-}$ (500 μM); (5) $CO_3^{2-}$ (500 μM); (6) $SO_4^{2-}$ (500 μM); (7) $NO_3^-$ (500 μM); (8) $Na^+$ (500 μM); (9) $K^+$ (500 μM); (10) $Mg^{2+}$ (200 μM); (11) $Ca^{2+}$ (200 μM); (12) $Zn^{2+}$ (200 μM); (13) GSH (1 mM); (14) $H_2O_2$ (50 μM); (15) $ClO^-$ (50 μM); (16) $^{\bullet}OH$ (50 μM). (F) (1) blank; (2) $HSO_3^-$ (50 μM); (3) $HPO_4^{2-}$ (500 μM); (4) $PO_4^{3-}$ (500 μM); (5) $CO_3^{2-}$ (500 μM); (6) $SO_4^{2-}$ (500 μM); (7) $NO_3^-$ (500 μM); (8) $Na^+$ (500 μM); (9) $K^+$ (500 μM); (10) $Mg^{2+}$ (200 μM); (11) $Ca^{2+}$ (200 μM); (12) $Zn^{2+}$ (200 μM); (13) GSH (1 mM); (14) $H_2O_2$ (50 μM); (15) $ClO^-$ (50 μM); (16) $^{\bullet}OH$ (50 μM).

We subsequently investigated the capability of selectively monitoring $ONOO^-$ and $SO_2$ in living cells. As illustrated in Fig. 3, different substances were introduced into NP69 cells to alter the concentrations of $ONOO^-$ and $SO_2$. When 3-morpholino-sydnonimine (SIN-1, 50 μM), a $ONOO^-$ generator, was added to the cells and pre-treated for 1 h, the red ($ONOO^-$) channel fluorescence signal was significantly higher than in the control group, while the blue ($SO_2$) fluorescence remained

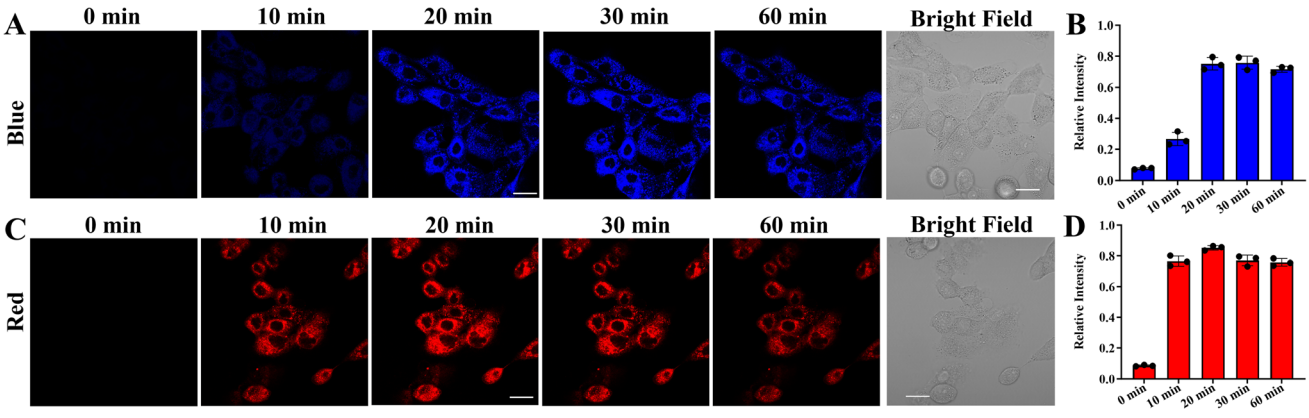


Fig. 2 Visualization of $ONOO^-$ and $SO_2$ in NP69 Cells. (A) Fluorescence imaging using probes after adding exogenous $SO_2$ to NP69 cells. (B) Statistical chart of average fluorescence intensity in figure (A). (C) Fluorescence imaging using probes after adding exogenous $ONOO^-$ to NP69 cells. (D) Statistical chart of average fluorescence intensity in figure (C). $\lambda_{ex/em}$ = 405/430–470 nm (blue channel), $\lambda_{ex/em}$ = 488/560–620 nm ($ONOO^-$ channel). Data are shown as mean ± S.D. Scale bar: 40 μm.

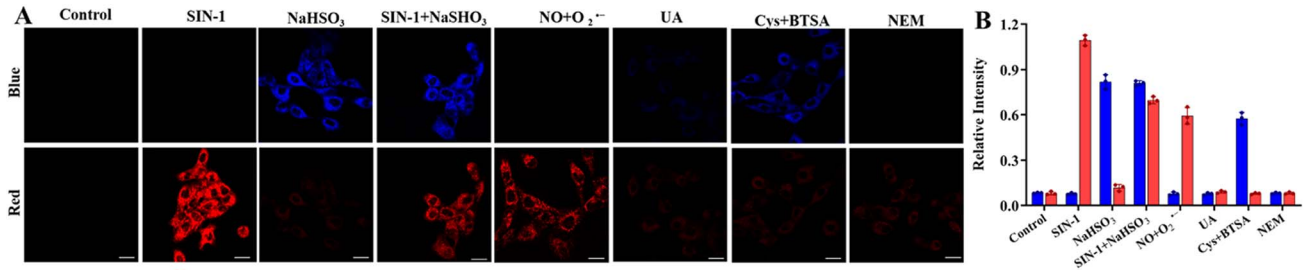


Fig. 3 The probe monitors intracellular $ONOO^-$ and $SO_2$ fluctuations.(A) Fluorescence imaging using probes after different substance pretreatments of NP69 cells: Group SIN-1, $NaHSO_3$, SIN-1+$NaHSO_3$, NO + $O_2^{\bullet-}$, and Cys + BTSA (pre-treated with $NaHSO_3$ (50 μM, 1 h),SIN-1 (50 μM, 1 h), $NaHSO_3$ (50 μM, 1 h), NO (50 μM, 1 h) + $O_2^{\bullet-}$ (50 μM 1 h), and Cys (50 μM 1 h) + BTSA (40 μM, 1 h) respectively). Group UA: pretreated with NO (50 μM) and $O_2^{\bullet-}$ (50 μM) for 1 hour, then treated with UA (500 μM) for 1 hour, followed by probe incubation for 10 min for imaging. Group NEM was pre-treated with Cys (50 μM) and BTSA (40 μM) for 1 hour, then treated with NEM (100 μM) for 1 h, followed by probe incubation for 10 minutes for imaging. (B) Statistical chart of average fluorescence intensity in figure (A). $\lambda_{ex/em}$ = 405/430–470 nm (blue channel), $\lambda_{ex/em}$ = 488/560–620 nm ($ONOO^-$ channel). Data are shown as mean ± S.D. Scale bar: 40 μm.

almost unchanged. This indicates that our probe can detect exogenous $ONOO^-$. When sodium hydrosulfite ($NaHSO_3$, 50 μM), an $SO_2$ donor, was added to NP69 cells and pre-treated for 1 h, the blue ($SO_2$) channel fluorescence was significantly higher than in the control group, with faint red ($ONOO^-$) channel fluorescence. After the simultaneous addition of SIN-1 and $NaHSO_3$ for the pre-treatment of NP69 cells, significant fluorescence was exhibited by both channels. These results demonstrate that HCy–$ONOO^-$–$SO_2$ enables the visual monitoring of $ONOO^-$ and $SO_2$ in cells. Nitric oxide and superoxide anion can generate $ONOO^-$ within cells. When NP69 cells were pre-treated with NO and superoxide anion, the red fluorescence signal of the $ONOO^-$ channel was significantly higher than in the control group. After using UA to neutralize the intracellular $ONOO^-$, the red fluorescence signal almost disappeared, further demonstrating that HCy–$ONOO^-$–$SO_2$ can detect the presence of endogenous $ONOO^-$ in cells. Previous studies have shown that sulfanilamide (BTSA) reacts with cysteine (Cys) to produce endogenous sulfur dioxide.[20] Therefore, we first the pre-treated cells with BTSA and Cys, then added the probe for imaging, obtaining a bright blue fluorescence signal. To verify whether this fluorescence signal was generated by $SO_2$, cells were treated with *N*-ethylmaleimide (NEM) for 0.5 h, followed by imaging with the probe (NEM group). We found that the blue fluorescence signal was almost imperceptible, indicating that HCy–$ONOO^-$–$SO_2$ can detect $SO_2$ in biological systems. These results demonstrate that HCy–$ONOO^-$–$SO_2$ can dynamically monitor $SO_2$ and $ONOO^-$ levels.

### 3.4. NO and $SO_2$ may reverse cisplatin resistance in nasopharyngeal carcinoma cells

Cisplatin is a first-line chemotherapeutic agent for nasopharyngeal carcinoma and typically demonstrates favourable efficacy in the treatment of early-stage disease. However, drug resistance significantly hinders its clinical application.

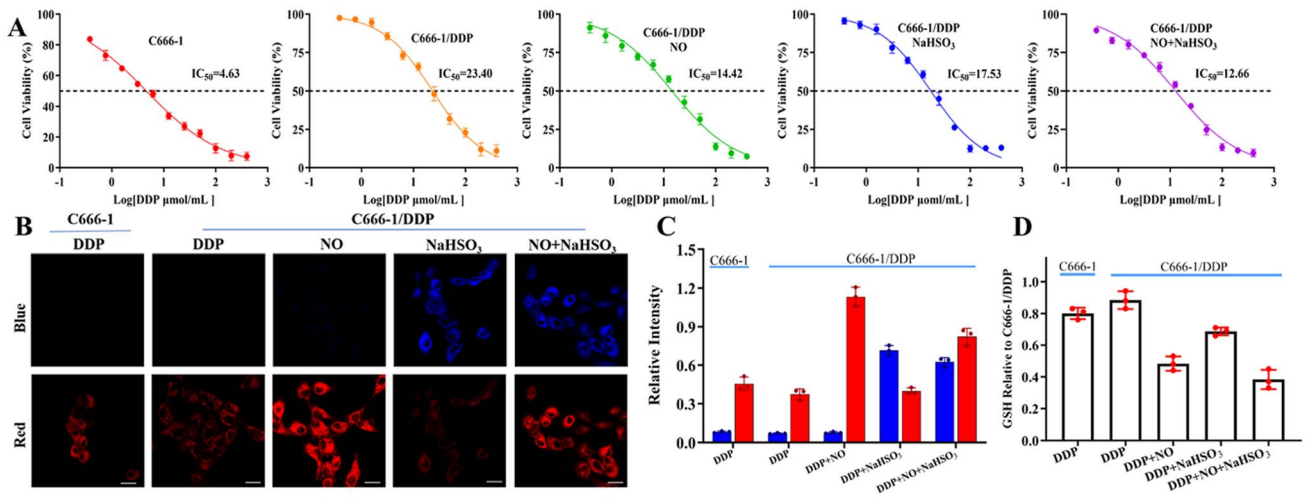


Fig. 4 NO and $SO_2$ reverse cisplatin resistance in nasopharyngeal carcinoma cells. (A) CCK-8 assay demonstrates NO and $SO_2$ resistance to C666-1/DDP cells. (B) Fluorescence probe analysis reveals the mechanism of NO and $SO_2$ resistance in C666-1/DDP cells. (C) Statistical chart of average fluorescence intensity in figure (B). (D) GSH assay detects intracellular GSH changes after NO and $SO_2$ treatment. $\lambda_{ex/em}$ = 405/430–490 nm (blue channel), $\lambda_{ex/em}$ = 488/560–620 nm (red channel). Data are presented as mean ± S.D. Scale bar: 40 μm.

Numerous cisplatin-resistant tumor models exhibit decreased reactive oxygen species (ROS) and elevated glutathione (GSH) levels. These findings have been further validated in clinical studies.[23–25] Recent research highlights the therapeutic potential of NO and $SO_2$. NO reacts with superoxide anion radicals to form highly reactive nitroxyl radicals ($ONOO^-$), which disrupt mitochondrial respiratory chains and induce dysfunction. $SO_2$ depletes GSH and disrupts redox balance in tumor cells, leading to increased ROS levels. We hypothesize that NO and $SO_2$ may counteract drug resistance by generating reactive nitrogen species (RNS) and depleting GSH. As shown in Fig. S13, we first ruled out the effects of trace NO and $SO_2$ on resistant cells. Subsequently, we pretreated cisplatin-resistant nasopharyngeal carcinoma cells (C666-1/DDP) with NO (20 μM) and $SO_2$ ($NaHSO_3$, 20 μM), then measured DDP $IC_{50}$ using CCK8 assay. Fig. 4A demonstrates that the $IC_{50}$ for cisplatin-sensitive cells (Group C666-1) was approximately 4.63 μmol $mL^{-1}$, whereas the $IC_{50}$ for resistant cells (Group C666-1/DDP) was 23.40 μmol $mL^{-1}$. Pretreatment with NO reduced the $IC_{50}$ of cisplatin in drug-resistant nasopharyngeal carcinoma cells was 14.42 μmol $mL^{-1}$, while pretreatment with $SO_2$ resulted in an $IC_{50}$ of 17.53 μmol $mL^{-1}$. Concurrent pretreatment with both NO and $SO_2$ reduced the $IC_{50}$ to 12.66 μmol $mL^{-1}$, significantly decreasing the required cisplatin dosage compared to the untreated group and reversing cisplatin resistance in nasopharyngeal carcinoma. Subsequent probe analysis of $ONOO^-$ and $SO_2$ levels in these groups showed that the red channel fluorescence signal increased markedly after NO treatment (Fig. 4B and C), indicating elevated intracellular $ONOO^-$ levels. The blue channel fluorescence signal also significantly intensified after $NaHSO_3$ treatment, suggesting elevated intracellular $SO_2$ levels. Notably, cisplatin-resistant cells exhibited lower $ONOO^-$ content than cisplatin-sensitive cells, which may be related to intracellular GSH levels. As shown in Fig. 4D, both NO and $NaHSO_3$ treatments significantly reduced intracellular GSH levels compared to the untreated group, with cisplatin-sensitive cells demonstrating lower GSH content than resistant cells. These results validated our hypothesis that NO and $SO_2$ induce RNS production and deplete intracellular GSH to counteract cisplatin resistance.

## 4. Conclusion

In summary, we designed and synthesized a small-molecule fluorescent probe, HCy–$ONOO^-$–$SO_2$, that responds to both $ONOO^-$ and $SO_2$. The probe had excellent stability and strong biocompatibility in complex biological systems, enabling the sensitive detection of changes in $ONOO^-$ and $SO_2$ within cells. Leveraging the probe's exceptional biochemical properties, we investigated the ability of NO and $SO_2$ to counteract cisplatin resistance in nasopharyngeal carcinoma, shedding light on their mechanisms. The results showed that NO and $SO_2$ can induce cisplatin resistance in nasopharyngeal carcinoma cells in a reversible manner by generating reactive nitrogen species and depleting glutathione. We believe that this probe has significant potential for evaluating the relationship between $NO/SO_2$ and cisplatin resistance and could provide a novel chemical tool for studying cisplatin resistance in nasopharyngeal carcinoma.

## Author contributions

Xiaofeng Wang: conceptualization, methodology, formal analysis, investigation, writing – original draft. Xinyu Li: data curation, validation, resources, software, visualization. Xiaoqiang Chen: supervision, project administration, writing – review & editing. Desheng Wang: supervision, conceptualization, writing – review & editing, funding acquisition.

## Conflicts of interest

We wish to confirm that there are no known conflicts of interest associated with this publication.

## Data availability

Data is provided within the manuscript or supplementary information (SI). Supplementary information: the general methods, reaction kinetics, and cell bright-field images, *etc.* See DOI: https://doi.org/10.1039/d5ra08282j.

## Acknowledgements

This work was supported by the 6th Batch of Cultivation Disciplines, Phase I (Category C) Construction Project (2025PYXKC02).

## References

1 Y.-P. Chen, A. T. C. Chan, Q.-T. Le, P. Blanchard, Y. Sun and J. Ma, Nasopharyngeal carcinoma, *Lancet*, 2019, **394**, 64–80.
2 F. Perri, G. Della Vittoria Scarpati, F. Caponigro, F. Ionna, F. Longo, S. Buonopane, *et al.*, Management of recurrent nasopharyngeal carcinoma: Current perspectives, *OncoTargets Ther.*, 2019, **12**, 1583–1591.
3 A. W. M. Lee, B. B. Y. Ma, W. T. Ng and A. T. C. Chan, Management of nasopharyngeal carcinoma: Current practice and future perspective, *J. Clin. Oncol.*, 2015, **33**, 3356–3364.
4 X. Sun, S. Liu, Y. Liang, Q. Chen, X. Li, L. Tang, *et al.*, The role of capecitabine as maintenance therapy in *de novo* metastatic nasopharyngeal carcinoma: A propensity score matching study, *Cancer Commun.*, 2020, **40**, 32–42.
5 L. Zhang, Y. Huang, S. Hong, Y. Yang, G. Yu, J. Jia, *et al.*, Gemcitabine plus cisplatin versus fluorouracil plus cisplatin in recurrent or metastatic nasopharyngeal carcinoma: A multicentre, randomised, open-label, phase 3 trial, *Lancet*, 2016, **388**, 1883–1892.
6 A. Prawira, S. F. Oosting, T. W. Chen, K. A. Delos Santos, R. Saluja, L. Wang, *et al.*, Systemic therapies for recurrent or metastatic nasopharyngeal carcinoma: A systematic review, *Br. J. Cancer*, 2017, **117**, 1743–1752.
7 S. S. Poh, Y. L. Soong, K. Sommat, C. M. Lim, K. W. Fong, T. W. Tan, *et al.*, Retreatment in locally recurrent

nasopharyngeal carcinoma: Current status and perspectives, *Cancer Commun.*, 2021, **41**, 361–370.
8 T. Fleihan, M. E. Nader and J. D. Dickman, Cisplatin vestibulotoxicity: A current review, *Front. Surg.*, 2024, **11**, 1437468.
9 M. Hesari, P. Mohammadi, M. Moradi, D. Shackebaei and F. Yarmohammadi, Molecular mechanisms involved in therapeutic effects of natural compounds against cisplatin-induced cardiotoxicity: A review, *Naunyn-Schmiedeberg's Arch. Pharmacol.*, 2024, **397**, 8367–8381.
10 B. Köberle, M. T. Tomicic, S. Usanova and B. Kaina, Cisplatin resistance: Preclinical findings and clinical implications, *Biochim. Biophys. Acta, Rev. Cancer*, 2010, **1806**, 172–182.
11 L. Kelland, The resurgence of platinum-based cancer chemotherapy, *Nat. Rev. Cancer*, 2007, **7**, 573–584.
12 M. Cavinato, Mitochondrial dysfunction and cisplatin sensitivity in gastric cancer: GDF15 as a master player, *FEBS J.*, 2024, **291**, 1111–1114.
13 V. Cocetta, E. Ragazzi and M. Montopoli, Mitochondrial involvement in cisplatin resistance, *Int. J. Mol. Sci.*, 2019, **20**, 3384.
14 L. Wu, J. Liu, X. Tian, R. R. Groleau, B. Feng, Y. Yang, *et al.*, Dual-channel fluorescent probe for the simultaneous monitoring of peroxynitrite and adenosine-5′-triphosphate in cellular applications, *J. Am. Chem. Soc.*, 2022, **144**, 174–183.
15 Y. Zhou, X. Yang, H. Lee, M. Yan and J. Yoon, Small-molecule fluorescent probes for detecting hydrogen peroxide in biological systems, *Coord. Chem. Rev.*, 2025, **541**, 216785.
16 N. W. Nkune, K. Moloudi, B. P. George and H. Abrahamse, An update on recent advances in fluorescent materials for fluorescence molecular imaging: A review, *RSC Adv.*, 2025, **15**, 22267–22284.
17 S. H. Alamudi and Y.-A. Lee, Design strategies for organelle-selective fluorescent probes: Where to start?, *RSC Adv.*, 2025, **15**, 2115–2131.
18 L. Odongo, G. Mulyowa, M. Goebeler and A. Trautmann, Bet v 1- and bet v 2-associated plant food sensitization in uganda and germany: Differences and similarities, *Int. Arch. Allergy Immunol.*, 2015, **167**, 264–269.
19 H. Mustroph, M. Stollenwerk and V. Bressau, Current developments in optical data storage with organic dyes, *Angew. Chem., Int. Ed.*, 2006, **45**, 2016–2035.
20 H. Cao, F. Yu, K. Dou, R. Wang, Y. Xing, X. Luo, *et al.*, Dual-response functionalized mitochondrial fluorescent probe for a double whammy monitoring of hypochlorite and sulfur dioxide in heat shock via time scales, *Anal. Chem.*, 2024, **96**, 18574–18583.
21 S. V. Mulay, Y. Kim, K. J. Lee, T. Yudhistira, H.-S. Park and D. G. Churchill, A fluorogenic and red-shifted diphenyl phosphinate-based probe for selective peroxynitrite detection as demonstrated in fixed cells, *New J. Chem.*, 2017, **41**, 11934–11940.
22 X. Luo, Z. Cheng, R. Wang and F. Yu, Indication of dynamic peroxynitrite fluctuations in the rat epilepsy model with a near-infrared two-photon fluorescent probe, *Anal. Chem.*, 2021, **93**, 2490–2499.
23 W. Yu, Y. Chen, N. Putluri, C. Coarfa, M. J. Robertson, V. Putluri, *et al.*, Acquisition of cisplatin resistance shifts head and neck squamous cell carcinoma metabolism toward neutralization of oxidative stress, *Cancers*, 2020, **12**, 1670.
24 Y. Han, W. Yin, J. Li, H. Zhao, Z. Zha, W. Ke, *et al.*, Intracellular glutathione-depleting polymeric micelles for cisplatin prodrug delivery to overcome cisplatin resistance of cancers, *J. Controlled Release*, 2018, **273**, 30–39.
25 N. K. Bejjanki, H. Xu and M. Xie, GSH triggered intracellular aggregated-cisplatin-loaded iron oxide nanoparticles for overcoming cisplatin resistance in nasopharyngeal carcinoma, *J. Biomater. Appl.*, 2021, **36**, 45–54.